Missing emissions from post-monsoon agricultural fires in northwestern India

Tianjia Liu[1,2], Miriam E. Marlier[3], Alexandra Karambelas[4], Meha Jain[5], Sukhwinder Singh[5], Manoj K. Singh[6], Ritesh Gautam[7], and Ruth S. DeFries[3]

[1]Department of Earth and Environmental Sciences, Columbia University, NY, USA
[2]Now at: Department of Earth and Planetary Sciences, Harvard University, Cambridge, MA, USA
[3]Department of Ecology, Evolution, and Environmental Biology, Columbia University, NY, USA
[4]The Earth Institute, Columbia University, New York, NY, USA
[5]School for Environment and Sustainability, University of Michigan, Ann Arbor, MI, USA
[6]School of Engineering, University of Petroleum and Energy Studies, Dehradun, Uttarakhand, India
[7]Environmental Defense Fund, Washington DC, USA

Corresponding author: Tianjia Liu (tianjialiu@g.harvard.edu)

Abstract

A rising source of outdoor emissions in northwestern India is crop residue burning, occurring after the monsoon (*kharif*) and winter (*rabi*) crop harvests. In particular, post-monsoon rice residue burning, which occurs annually from October to November and is linked to increasing mechanization, coincides with meteorological conditions that enhance short-term air quality degradation. Here we examine the Global Fire Emissions Database (GFED), whose bottom-up emissions are based on the 500-m burned area product, MCD64A1, derived from Moderate Resolution Imaging Spectroradiometer (MODIS) observations. Using a household survey from 2016, we find that MCD64A1 tends to underestimate burned area in many surveyed villages, leading to poor representation of small, scattered fires and consequent spatial biases in model results. To more accurately allocate such small fires and resolve within-village heterogeneity, we use an experimental hybrid MODIS-Landsat method (ModL2T) to map burned area at 30-m spatial resolution, which results in 44 ± 21% higher burned area than MCD64A1 and up to 105 ± 52% increase in dry matter emissions over GFEDv4s. In our validation and assessments, we find that ModL2T performs better relative to MCD64A1 in terms of bias and omission error, but may introduce commission error due to conflation of burning with harvest and still underestimate burned area due to Landsat's coarse temporal resolution (every 16 days). We conclude that while MODIS and Landsat provide more than two decades worth of observations, their spatio-temporal resolution is too coarse to overcome several region-specific challenges: small median landholding size (1-3 ha), quick harvest-to-sowing turnover period, prevalence of partial burning, and increasing haziness. To further constrain agricultural fire emissions in northwestern India and improve model estimates of associated public health impacts, integration of finer resolution imagery, as well as better understanding of the spatial patterns in burn rates, burn practices, and fuel loading, is requisite.

1 Introduction

India is embracing agricultural mechanization to increase crop productivity and decrease labor costs in order to feed its rapidly growing population (Mehta *et al* 2014). Agriculture in

India is currently only mechanized on 40-45% of cropland, below that of the United States, Russia, western Europe, China, and Brazil (57-95%) (Bai 2014, Mehta *et al* 2014). India's projected population surge from 1.3 billion in 2015 to 1.7 billion by 2050 demands sustainable increases in crop productivity, intensity, and yield, which in turn bolsters the rise of agricultural mechanization (United Nations 2015). Traditionally, farmers collect crop residue to feed livestock. However, as India mechanizes, farmers are using combine harvesters, which leave behind scattered crop residues that are labor intensive to remove (Vadrevu *et al* 2011, Kumar *et al* 2015). Gupta (2012) estimates that rice residues in 90% of area harvested by combine harvesters are burned in Punjab, in which emissions can severely degrade regional air quality seasonally (Gupta 2012, Kumar *et al* 2015, Liu *et al* 2018). However, the air quality impacts from agricultural fires remain highly uncertain due to differences in global fire emissions inventories that are coupled with atmospheric transport models (Cusworth *et al* 2018). Here we assess the challenges of using satellite observations to map burned area and active fires in order understand where current emissions estimates are most underestimated and uncertain.

In this study, we focus on the post-monsoon burning season in northwestern India. Previous work using satellite fire detections and HYSPLIT atmospheric back trajectories suggests that pre-monsoon (April-May) wheat residue burning is of less concern to the Delhi National Capital Region's air quality than post-monsoon (October-November) rice residue burning due to different atmospheric transport patterns, higher ventilation from high boundary layer conditions, and less overall fire intensity (Liu *et al* 2018). Smoke plumes from post-monsoon crop residue burning, primarily originating from agricultural states Punjab and Haryana, are transported across the densely-populated Indo-Gangetic Plain (IGP) (Figure 1). In general, carbonaceous particles in smoke can be transported hundreds of kilometers in the atmosphere (Sharma *et al* 2010, Kaskaoutis *et al* 2014). Besides air quality degradation and public health impacts, crop residue burning also inhibits the productivity of the next cropping season by reducing soil quality (Gupta *et al* 2004). However, the short timeframe to clear fields of rice residue and sow winter wheat is a key limiting factor, thus leading to increased combine harvester use and subsequent burning (Gupta 2012, Jain *et al* 2014). Thus, despite restrictions on agricultural burning, farmers continue to burn crop residue due to the lack of viable, well-incentivized, and cost-effective alternatives.

In this study, we first quantify the range of post-monsoon agricultural fire emissions estimates from five inventories for Punjab and Haryana, from 2003-2016. Specifically, we assess the region-specific challenges of estimating fire activity using satellite-derived burned area and active fire products, which are used as input in emissions inventories. We then develop a hybrid MODIS-Landsat method to experimentally downscale post-monsoon agricultural burned area from 500-m to 30-m spatial resolution. Next, we validate burned area estimates using household survey data and make further assessments using 375-m Visible Infrared Imaging Radiometer Suite (VIIRS) active fire detections and MODIS aerosol optical depth (AOD). We evaluate active fire products using fine-resolution (<5 m) imagery. Finally, we discuss crop residue burning practices in northwestern India in the context of policy changes and increasing mechanization and land fragmentation.

2 Data and methods

2.1. Overview of study area and satellite-derived datasets

The study area consists of two neighboring agricultural states in northwestern India, Haryana and Punjab (Figures 1, S1). Punjab and Haryana are situated at the heart of India's "bread basket," where most farmers predominantly follow a rice-wheat rotation.

Table S1 summarizes the satellite-derived surface reflectance, fire, and land cover datasets, primarily from MODIS and Landsat, used in this study. We use Google Earth Engine (GEE), a cost-free, petabyte-scale cloud computing platform, to retrieve datasets and for geospatial analysis (Gorelick *et al* 2017). We also survey five global fire emissions inventories, spanning a range of "bottom-up" burned area-based and "top-down" fire energy-based methods, to evaluate differences in agricultural fire emissions over the study region: (1) Global Fire Emissions Database (GFEDv4s; van der Werf *et al* 2017), (2) Fire Inventory from NCAR (FINNv1.5; Wiedinmyer *et al* 2011), (3) Global Fire Assimilation System (GFASv1.2; Kaiser *et al* 2012), (4) Quick Fire Emissions Dataset (QFEDv2.5; Darmenov and da Silva 2013), and (5) Fire Energetics and Emissions Research (FEERv1.0-G1.2; Ichoku and Ellison 2014). Each inventory is described is more detail in appendix S1.3.

2.2. Burned area and active fires: validation and assessments

2.2.1. Burned area

Previous studies on high-resolution agricultural burned area estimation in northwestern India span 1-2 years of study (PRSC 2015, Yadav *et al* 2014a, 2014b). Here we use GEE to expand the study time period to 14 years, from 2003-2016, and estimate the total extent of post-monsoon agricultural burned area at 30-m spatial resolution, improving on "baseline" 500-m MODIS MCD64A1 burned area with better spatial allocation of small fires. Here we primarily focus on burned area, because Landsat has no active fire product. Our hybrid MODIS-Landsat method is a simplified version of the MCD64A1 global burn mapping algorithm and GFEDv4s small fires boost approach of integrating active fires as training data (Giglio *et al* 2009, Randerson *et al* 2012). MODIS 1-km active fire locations represent endmembers of larger clusters of small fires from which we can obtain the spectral signature and apply to Landsat at higher resolution. ModL2T is described in more detail in appendix S2. Figure S3 describes the workflow for the ModL2T algorithm, which can be summarized as follows: (1) pre-process individual scenes; (2) composite cloud-free scenes in pre-fire and post-fire collections; (3) define thresholds based on the quantile intersection of normalized burn ratio (NBR), a metric used extensively in burn scar mapping, in burned and unburned agricultural areas; (4) separately derive MODIS and Landsat burned area using NBR thresholds; and (5) merge Landsat and MODIS classifications and apply an agricultural mask.

We independently validate burned area by using a 2016 household survey on farm management practices across the IGP. The survey asks participants whether crop residue is burned before planting wheat. Because the survey responses inherently distinguish between burned and unburned fields, this validation addresses the conflation of burning with harvest. We use 1112 responses from farmers in 30 Punjab and 32 Haryana villages, spanning eight districts. Because the GPS coordinates associated with each response are not located in-field, we cannot match responses to individual fields. We thus group responses by village name and match mean

GPS coordinates with an accuracy <10 m to village shapefiles. On average, 18 ± 5 households were surveyed per village. We normalize the % households that burned crop residue by approximate operated landholding area. We do not account for partial burns and assume a field is entirely burned if a farmer affirms crop residue burning. For comparison, we estimate the % BA_{ModL2T} and $BA_{MCD64A1}$ of total village cultivated area based on 30-m GlobeLand30 and 500-m MODIS MCD12Q1 land cover, respectively. Due to these normalized approximations spurred by data limitations, the two metrics of % burning per village are not directly comparable on a 1:1 basis. We further assess $BA_{MCD64A1}$ and BA_{ModL2T} with simple checks using: (1) higher resolution active fire locations from VIIRS (pixel-level), (2) previous burned area estimates (district-level) and (3) satellite AOD (region-level). These assessments and their caveats are described in detail in appendix S3.4.

We next estimate the maximum relative increase in GFEDv4s agricultural dry matter (DM) emissions by using ModL2T and MCD64A1 C6 burned area; DM emissions can be converted to other chemical species (e.g. CO_2, CO, OC, BC) using emissions factors (Akagi *et al* 2011). While DM emissions are often calculated using estimates of fuel loading and combustion completeness in addition to burned area in bottom-up approaches, we exploit the highly linear GFEDv4s DM/BA slope for each 0.25° x 0.25° grid cell to directly scale BA to DM (appendix S4).

2.2.2. Active fires

We use Google Earth's sparse collection of fine-resolution (<5 m) historical imagery (DigitalGlobe and CNES/Airbus) to validate the MxD14A1 active fire product. Using all publicly available DigitalGlobe and CNES/Airbus imagery, we estimate omission error using >500 identified ignition hotspots, spanning >400 1-km pixels, for 34 different days over Oct-Nov, 2010-2016; we can pinpoint these active fires by tracing smoke plumes back to individual fields. We also categorize each ignition as a complete or partial burn to assess variations in satellite detection of fires related to the method of burning. We define complete burns as burn scars that extend across entire fields in which both intact and loose residues are burned and partial burns as circular or ring-shaped burn scars often located in the center of fields, where loose residues are stacked. We can then assign a date to the in-progress fires based on the scene acquisition date, adjusted to local time, and determine whether MODIS indeed detected these fires on the same day.

Finally, we assess the capability of INSAT-3D, a geostationary satellite that provides active fire counts every 30 minutes since October 2013, to map post-monsoon agricultural fires despite its coarse 4-km spatial resolution.

2.3. Landholdings and mechanization

We consider ancillary data on landholdings and combine harvester use to assess trends in land fragmentation and mechanization. The Indian Department of Agriculture, Cooperation, and Farmers Welfare conducts the agricultural census and provides two online quinquennial databases: Agricultural Census and Input Survey. The Agricultural Census database, which is based on census and input sample survey data, includes detailed data on landholdings in India from 1995-96 to 2010-11 (http://agcensus.dacnet.nic.in/); the Input Survey database contains information on agricultural implements and machinery, including combine harvesters, from 1996-97 to 2011-12 (http://inputsurvey.dacnet.nic.in/). In addition, the 2016 household survey asks participants about rice harvesting methods. Response choices include: fully mechanical (e.g. combine harvester), partially mechanical (e.g. thresher), and manually. We exclude 140 responses from farmers who never harvested rice.

3 Results

3.1. Spatio-temporal distributions in fire activity

Following Vadrevu *et al* (2011), we use the 1-km combined MODIS/Terra and Aqua active fire counts (MCD14ML) to show average annual timing of pre-monsoon (April-May) and post-monsoon (October-November) fire activity, from 2003-2016 (Figure 2a). We put this in context of the rice-wheat rotation in northwestern India, which we show as variations in greenness estimated from MODIS MOD09A1 8-day composite NBR. Whereas high NBR represents peak growth of the monsoon crop during late February to early March and winter crop during late August to early September, low NBR is associated with bare soil and burn scars post-harvest and after crop residue burning. MCD64A1 burn frequency shows repeated post-monsoon fire activity from 2003-2016, particularly in southern-central Punjab (Figure 2b), where fires occur later in the fire season than in northern Punjab (Figure 2c). In addition, Aqua (1:30 pm local time, daytime overpass) averages 647 ± 293% higher in fire counts than Terra (10:30 am) during the 2003-2016 post-monsoon burning seasons, which is consistent with the early to late afternoon peak fire energy (Figure S6, appendix S3.2).

3.2. Quantification of post-monsoon fire activity

Current inventory estimates of post-monsoon fire emissions over Punjab and Haryana are highly variable at 74-107% in coefficient of variation and range from 12-119 Tg OC+BC (Table 1). The order-of-magnitude higher emissions from FEERv1.0-G1.2 is influenced by its top-down calculation of aerosol emissions using smoke AOD observations, whereas bottom-up inventories, such as GFEDv4s and FINNv1.5, depend heavily on satellite fire observations (Ichoku and Ellison 2014, van der Werf *et al* 2017, Wiedinmyer *et al* 2011). While the two other top-down inventories, GFASv1.2 and QFEDv2.5, adjust for unobserved fires obscured by clouds, both calibrate emissions using GFEDv4s, which may explain the low bias in these two inventories (Kaiser *et al* 2012, Darmenov and da Silva 2013).

3.2.1. Validation and assessments of MCD64A1 and ModL2T burned area

Post-monsoon BA_{ModL2T} is on average 44 ± 21% higher than $BA_{MCD64A1}$ in Punjab and Haryana from 2003-2016 (Figure 3, Table S4). We estimate 45-72% of BA_{ModL2T} with good confidence (score ≥ 3) and 16-36% for experimental Landsat-only BA_{ModL2T} boost (score = 2) (Figure S5). Proportionally, $BA_{MCD64A1}$ in Haryana constitutes a smaller fraction (14 ± 3%) of total burned area in the study region than BA_{ModL2T} (26 ± 3%). This indicates that the increase in burned area from ModL2T over MCD64A1 is driven by additional burn scar detections in Haryana. Using the strongly linear relationship between GFEDv4s BA and agricultural dry matter (DM) emissions, we estimate that using C6 MCD64A1 and ModL2T burned area increases post-monsoon GFEDv4s DM emissions by 44 ± 22% and 105 ± 52%, respectively, from 2003-2016 (Figure S13).

We independently validate burned area with household survey data from 2016. We compare post-monsoon village-level survey crop residue burning rates, normalized by total landholding area, with $BA_{MCD64A1}$ and BA_{ModL2T} expressed as a fraction of cropland area. The village-level fraction of surveyed households that burn crop residue is moderately correlated with fractional BA_{ModL2T} (r = 0.67, p < 0.05) (Figures 3c, 4a). ModL2T underestimates burn rates for villages with high fractional burn rates (0.9-1), which may be partly due to partial burning and uncertainties in agricultural area mapped by GlobeLand30 (Figure 4b). $BA_{MCD64A1}$ achieves a weaker correlation of r = 0.6 (p < 0.05) with higher normalized mean bias and severe underestimates in burned area for many villages, skewing its distribution toward low fractional burn rates (Figure S7).

We assess omission and maximum commission errors based on the co-location of VIIRS active fire detections with $BA_{MCD64A1}$ and BA_{ModL2T}, from 2012-2016. With a higher spatial resolution (375 m) than MODIS/Terra and Aqua (1 km), VIIRS more consistently detects smaller and cooler fires (Figure S8). We find that BA_{ModL2T} yields a lower omission error (1-8%) than $BA_{MCD64A1}$ (33-46%) (Table S4). The maximum commission error is much higher for BA_{ModL2T} (43-55%) than $BA_{MCD64A1}$ (10-19%), but may reflect undetected active fires outside VIIRS overpasses or those obscured by thick haze or clouds. In particular, $BA_{MCD64A1}$ is often unable to detect active fire hotspots in regions with prevalent partial burning, such as in central Haryana and northern Punjab (Figures 3b, 4, S8). Over the 5-year period from 2012-2016, VIIRS detected active fires in 68% of the 0.02° grid cells in Punjab and Haryana, while MODIS only detected active fires in 54% of the area (Figure S4c). In addition, VIIRS detected that 41% of grid cells burned consecutively from 2012-2016, while MODIS detected only 14% of grid cells by this criterion.

Next, we compare district-level burned area with previous estimates (PRSC 2015; Yadav *et al* (2014a; 2014b). Overall, total Punjab BA_{ModL2T} is 6% lower and 7% higher than that of PRSC (2015) in 2014 and 2015, respectively. In contrast, Punjab $BA_{MCD64A1}$ is lower than PRSC (2015) burned area estimates in both 2014 and 2015 by 19% and 2%, respectively (Figure S9). For northern Haryana districts, both ModL2T and MCD64A1 tend to overestimate burned area relative to Yadav *et al* (2014a; 2014b). District-level BA_{ModL2T} and $BA_{MCD64A1}$ are strongly correlated (r = 0.87-0.88, p < 0.05) with previous burned area estimates. In terms of mean absolute error, ModL2T (251 km^2) outperforms MCD64A1 (282 km^2). However, MCD64A1 (slope = 1.04 ± 0.08) shows less overall bias than ModL2T (slope = 0.89 ± 0.07).

Finally, we assess detrended interannual variations in mean post-monsoon MODIS AOD and BA_{ModL2T}. Similar to daily FRP-AOD relationship quantified in Liu *et al* (2018), we find that regional BA_{ModL2T} is weakly positively correlated with mean regional AOD (r = 0.46, p = 0.1), but not statistically significant (Figure S10a). Comparatively, $BA_{MCD64A1}$ is unexpectedly anti-correlated with AOD (r = -0.54, p < 0.05) (Figure S10b).

3.3. Validation of active fires with fine-resolution imagery: two burning practices

Two main crop residue burning practices are observed in Punjab and Haryana: complete and partial burns (Gupta 2012, Kumar *et al* 2015). Although farmers employ a mixture of the two practices, mapped active ignitions from available fine-resolution imagery show that complete burns are widespread in Punjab and northern Haryana, while partial burns are more pervasive in central and southeast Haryana (Figure 3b). Complete burns induce dark scarring over entire fields such that adjoining fields burned in this way within days of each other are starkly contrasted against the surrounding unburned landscape (Figure 5a). Partial burns leave small, circular or ring-shaped scarring in the center of fields; only ~1/9 of the field area is scarred

(Figure 5b). We find that the MODIS active fire product poorly matches in-progress fires identified from available fine-resolution imagery. Same-day omission error is 95%, with all co-locations from complete burns (Table 2). Same-season omission error decreases to 75%, suggesting active fires within the same 1-km pixel were detected on other days.

3.4. Trends in landholding size, combine harvesters, and agricultural burning

The median landholding size in Haryana (1-2 ha) is smaller than that in Punjab (2-3 ha) (Figure S14). After some consolidation of small landholdings from 1995-96 to 2000-01, landholdings became increasingly fragmented from 2000-01 to 2010-11. From 1996-97 to 2011-12, the number of combine harvesters increased over 20-fold from 14,664 to 297,132 in Haryana and almost 3-fold from 93,191 to 256,162 in Punjab. Based on the 2016 household survey, 72% of farmers using a combine harvester to harvest rice subsequently burned the crop residue in preparation for sowing wheat in Punjab and Haryana, compared to manual harvesting (8%) (Table 3). Mechanization is less strongly linked to burning in Haryana, where only 32% of farmers using combine harvesters burn rice residue, compared to 87% in Punjab. Overall, of those who burned rice residue, 98% had used fully or partially mechanical methods of harvesting.

Overall, BA_{ModL2T} increased by 966 ± 179 $km^2\ yr^{-1}$ ($p < 0.05$), or 82% in total, from 2003-2016 (Figure S10c). While increased Landsat scene availability (Figure S2) may account for the some of the upward trend in BA_{ModL2T}, the upward trend in $BA_{MCD64A1}$, which has no dependency on Landsat, is higher at 974 ± 85 $km^2\ yr^{-1}$ ($p < 0.05$), or 142% in total. Over the same 14-year time period, mean Oct-Nov satellite AOD increased by 39% in total, or 0.017 ± 0.003 yr^{-1} ($p < 0.05$) (Figure S10d); increased aerosol loading during the post-monsoon is also apparent from ground-based column AOD measurements from the Aerosol Robotic Network (AERONET) site at Lahore (in the neighboring Pakistan province of Punjab) (Figure S11).

4 Discussion

4.1. MCD64A1 and ModL2T burned area: validation, assessments, and uncertainties

In northwestern India, increasing rates of post-monsoon agricultural burning enhance downwind air quality degradation and are linked to more widespread use of mechanized harvesting methods. Emissions estimates for agricultural fires in northwestern India are poorly constrained, on average ranging from 12-119 Tg OC+BC over the post-monsoon burning period among five inventories. In this study, we target the MODIS-derived burned area estimates used as input in GFEDv4s. MCD64A1, a primary input in GFEDv4s, is known to perform poorly in various agricultural regions (Giglio 2015, Hall *et al* 2016, Zhu *et al* 2017, Lasko *et al* 2017, Fornacca *et al* 2017). We combine MODIS and Landsat imagery to experimentally improve the spatial allocation of post-monsoon agricultural burned area in northwestern India for 14 years from 2003-2016. Use of Landsat imagery has been primarily limited by: (1) its low temporal resolution (16 days) and (2) storage and computing power. To minimize these limitations, we implement a hybrid MODIS-Landsat approach in GEE to rapidly process large collections of MODIS and Landsat imagery and expand the spatio-temporal range of study. Our simplified methodology is subject to several limitations, such as inconsistent Landsat availability, averaging of NBR across Landsat platforms, region-averaged NBR thresholds, and assumption that timing of the crop cycle is relatively homogeneous. Nevertheless, we find that incorporating Landsat imagery can improve the spatial allocation of small fires in northwestern India, which is important for modeling studies in which small fire emissions in close proximity to population centers can significantly impact local air quality estimates.

In comparison to MCD64A1, the ModL2T algorithm estimates on average 44 ± 21% higher burned area in Haryana and Punjab during post-monsoon, from 2003-2016. ModL2T allocates burned area for partial burns in Haryana that are largely unaccounted for in MCD64A1. Validation of burned area with household survey data in 2016 suggests that the ModL2T algorithm can estimate burned area with increased accuracy (r = 0.67, NMB = -25.7%), compared to MCD64A1 (r = 0.6, NMB = -28.6%). In additional assessments, we find that BA_{ModL2T} improves on $BA_{MCD64A1}$ in terms of omission error, comparison with previous estimates of burned area, and relationship with satellite AOD, but may introduce commission errors (appendix S3.4).

4.2. Limitations of burned area and active fire algorithms in northwestern India

We identify several key limitations that make the spatio-temporal resolution of MODIS, Landsat, VIIRS, and INSAT-3D insufficient for detecting active fires and accurately mapping cropland burned area in northwestern India: (1) prevalence of partial burning, (2) small landholding sizes and increasing fragmentation, (3) short duration of fires, (4) possible commission error from conflation of burning with harvest, (5) quick harvest-to-sowing period lead to missed fires, and (6) increasing haziness that limits satellite observing area.

Based on the two dominant types of burning practices in Punjab and Haryana, partial burning, which is prevalent in central and southern Haryana, may be more difficult to detect due to sub-landholding size fires. This difficulty is compounded by small median landholding sizes in Haryana (1-2 ha) and Punjab (2-3 ha). The inability of MODIS to readily detect partial burns and its tendency to homogenize over clusters of fields means that GFED4s grid cells with mostly partial burning are likely to contain a small sample of small fires, or none. This implies that the potential of the GFEDv4s small fires boost is limited in these areas in particular, and that the spatial allocation of these small fires is also not well-represented.

The GFEDv4s small fire boost relies on active fire hotspots and dNBR-based ratios from 16-day MODIS surface reflectance composites (Randerson *et al* 2012). This methodology assumes a linear correlation of burn severity with burned area. However, unlike wildfires, whose burn severity and burned area extent can vary greatly, cropland fires are generally controlled in burn rate, time, and area, thus limiting the upper bound of burn severity and burned area extent per fire. For cropland fires, dNBR has been used more as a threshold for burned area classification rather than a proxy for burn severity (e.g. McCarty *et al* 2008, 2009, Oliva and Schroeder 2015, Zhu *et al* 2017, Zhang *et al* 2018). However, the decline in NBR at the end of the growing season is influenced by both harvest and burning (Hall *et al* 2016). Clearly attributing decreases in NBR to burning remains challenging due to noise in the daily NBR timeseries. Further, the limited harvest-to-sowing turnaround period during post-monsoon means that burning may immediately follow harvest (Kumar *et al* 2015); we find that burn scars can disappear as soon as within several days. The low temporal availability of Landsat further increases its susceptibility to low pixel availability from haze and clouds, possibly leading to large mismatches in the satellite acquisition date between neighboring scenes. We conclude that both Landsat and MODIS surface reflectance products (8-day and 16-day) are fundamentally too temporally coarse to accurately classify burned area.

Unlike burned area, active fires are derived from thermal anomalies and thus not susceptible to conflation of burning with harvest. However, detection of small, short-lasting fires is greatly hindered by coarse spatio-temporal resolution. In India, agricultural fires typically last no more than half an hour (Thumaty *et al* 2015). We find an omission error of >90% by the MODIS active fires product. VIIRS, at a higher 375-m spatial resolution, detected ~20% more 0.02° grid cells with active fires than MODIS/Terra and Aqua, from 2012-2016. Even so, VIIRS would not be able detect fires obscured by haze and those outside of its overpass time. Li *et al* (2018) showed that even slight differences in VIIRS and MODIS/Aqua overpasses of ~15 minutes can lead to large discrepancies in active fire detections over Punjab. In addition, cloud cover and increasing haziness, indicated by AOD, can limit retrieved scenes that are usable and block active fires from satellite detection. The short return time (30 minutes) of INSAT-3D makes it ideal for capturing short-lasting agricultural fires, but its coarse 4-km spatial resolution makes INSAT-3D unable to detect such fires (Figure S12).

4.3. Future directions for improving agricultural fire emissions

The recent proliferation of finer resolution satellites, such as S-NPP (375 m and 750 m, daily, post-2012), Sentinel-2 (10-20 m, every 5 days, post-2015) and Planet (<5 m, daily, post-2016), offers added potential for active fire and burn scar detection (Drusch *et al* 2012, Strauss 2017). For more recent years of study, these higher resolution imagery can help constrain the spatial and temporal variability of agricultural fire emissions in northwestern India. In particular, partial burns are difficult to detect at MODIS and Landsat resolution, but discernable with fine-resolution imagery. In addition, the present inability of moderate-resolution sensors to detect partial burns also raises the question of how end-users of fire emissions inventories should account for these missing emissions. More detailed on-the-ground knowledge of the amount of crop residues generated, as well as burn rates and practices, is needed to inform inventories retroactively. Differences in burn scar area from complete and partial burns also imply that separate fuel loading estimates are needed for bottom-up approaches. Additional uncertainty in post-monsoon smoke OC+BC emissions, which differ by an order of magnitude among five widely-used inventories, signals a need to evaluate not only the satellite fire input products used, but also differences in statistical boosts applied, emissions factors, and fuel consumption estimates for croplands in northwestern India. Based on the underestimation of emissions from agricultural fires in this region, it is likely that atmospheric models using available active fire and burned area products considerably underestimate smoke exposure and public health impacts from these fires. Future collaborations to incorporate accurate estimates of emissions can provide more robust input for policy decisions.

Acknowledgements

We acknowledge the Columbia University Department of Earth and Environmental Sciences Young Investigator Award and Earth Institute Research Assistantship program for support for this work, as well as the Columbia University President's Global Innovation Fund. This work was also supported by a National Science Foundation Graduate Research Fellowship awarded to T.L. (Award Number DGE1144152 and DGE1745303). The household survey in 2016 was funded by a NSF SEES Postdoctoral Fellowship (Award Number 1415436) to M.J. We also thank Dr. Brent Holben and site managers for establishing and maintaining AERONET Lahore, Pakistan site. We thank Dr. Loretta Mickley for helpful comments regarding this manuscript.

References

Akagi S K, Yokelson R J, Wiedinmyer C, Alvarado M J, Reid J S, Karl T, Crounse J D and Wennberg P O 2011 Emission factors for open and domestic biomass burning for use in atmospheric models *Atmos. Chem. Phys.* **11** 4039–72

Bai R 2014 *Analysis of the Trends of Agricultural Mechanization Development in China (2000-2020). CSAM Policy Brief.* Online: http://www.un-csam.org/publication/PB201401.pdf

Cusworth D H, Mickley L J, Sulprizio M P, Liu T, Marlier M E, DeFries R S, Guttikunda S K and Gupta P 2018 Quantifying the influence of agricultural fires in northwest India on urban air pollution in Delhi, India *Environ. Res. Lett.* **13** 044018 Online: https://doi.org/10.1088/1748-9326/aab303

Darmenov A S and da Silva A 2013 *The Quick Fire Emissions Dataset (QFED) - Documentation of versions 2.1, 2.2, and 2.4* vol 32, ed M J Suarez Online: http://citeseerx.ist.psu.edu/viewdoc/summary?doi=10.1.1.406.7724

Drusch M, Del Bello U, Carlier S, Colin O, Fernandez V, Gascon F, Hoersch B, Isola C, Laberinti P, Martimort P, Meygret A, Spoto F, Sy O, Marchese F and Bargellini P 2012 Sentinel-2: ESA's Optical High-Resolution Mission for GMES Operational Services *Remote Sens. Environ.* **120** 25–36 Online: https://doi.org/10.1016/j.rse.2011.11.026

Fornacca D, Ren G and Xiao W 2017 Performance of Three MODIS fire products (MCD45A1, MCD64A1, MCD14ML), and ESA Fire_CCI in a mountainous area of Northwest Yunnan, China, characterized by frequent small fires *Remote Sens.* **9** 1–20 Online: https://doi.org/10.3390/rs9111131

Giglio L 2015 *MODIS Collection 6 Active Fire Product User's Guide Revision A* Online: https://cdn.earthdata.nasa.gov/conduit/upload/3865/MODIS_C6_Fire_User_Guide_A.pdf

Giglio L, Loboda T, Roy D P, Quayle B and Justice C O 2009 An active-fire based burned area mapping algorithm for the MODIS sensor *Remote Sens. Environ.* **113** 408–20 Online: https://doi.org/10.1016/j.rse.2008.10.006

Gorelick N, Hancher M, Dixon M, Ilyushchenko S, Thau D and Moore R 2017 Google Earth Engine: Planetary-scale geospatial analysis for everyone *Remote Sens. Environ.* **202** 18–27 Online: https://doi.org/10.1016/j.rse.2017.06.031

Gupta P K, Sahai S, Singh N, Dixit C K, Singh D P, Sharma C, Tiwari M K, Gupta R K and Garg S C 2004 Residue burning in rice–wheat cropping system: Causes and implications *Curr. Sci.* **87** 173–209 Online: https://www.jstor.org/stable/24109770

Gupta R 2012 *Causes of Emissions from Agricultural Residue Burning in North-West India: Evaluation of a Technology Policy Response* Online: http://www.sandeeonline.org/uploads/documents/publication/962_PUB_Working_Paper_66_Ridhima_Gupta.pdf

Hall J V., Loboda T V., Giglio L and McCarty G W 2016 A MODIS-based burned area assessment for Russian croplands: Mapping requirements and challenges *Remote Sens. Environ.* **184** 506–21 Online: http://dx.doi.org/10.1016/j.rse.2016.07.022

Ichoku C and Ellison L 2014 Global top-down smoke-aerosol emissions estimation using satellite fire radiative power measurements *Atmos. Chem. Phys.* **14** 6643–67 Online:

https://doi.org/10.5194/acp-14-6643-2014

Jain N, Bhatia A and Pathak H 2014 Emission of air pollutants from crop residue burning in India *Aerosol Air Qual. Res.* **14** 422–30 Online: https://doi.org/10.4209/aaqr.2013.01.0031

Kaiser J W, Heil A, Andreae M O, Benedetti A, Chubarova N, Jones L, Morcrette J J, Razinger M, Schultz M G, Suttie M and van der Werf G R 2012 Biomass burning emissions estimated with a global fire assimilation system based on observed fire radiative power *Biogeosciences* **9** 527–54 Online: https://doi.org/10.5194/bg-9-527-2012

Kaskaoutis D G, Kumar S, Sharma D, Singh R P, Kharol S K, Sharma M, Singh A K, Singh S, Singh A and Singh D 2014 Effects of crop residue burningonaerosol properties, plume characteristics, and long-range transport over northern India *J. Geophys. Res. Atmos.* **119** 5424–44 Online: https://doi.org/10.1002/2013JD021357

Kumar P, Kumar S and Joshi L 2015 *Socioeconomic and Environmental Implications of Agricultural Residue Burning* Online: https://doi.org/10.1007/978-81-322-2014-5

Lasko K, Vadrevu K P, Tran V T, Ellicott E, Nguyen T T N, Bui H Q and Justice C 2017 Satellites may underestimate rice residue and associated burning emissions in Vietnam *Environ. Res. Lett.* **12** Online: https://doi.org/10.1088/1748-9326/aa751d

Li F, Zhang X, Kondragunta S and Csiszar I 2018 Comparison of Fire Radiative Power Estimates From VIIRS and MODIS Observations *J. Geophys. Res. Atmos.* **123** 4545–63 Online: https://doi.org/10.1029/2017JD027823

Liu T, Marlier M E, DeFries R S, Westervelt D M, Xia K R, Fiore A M, Mickley L J, Cusworth D H and Milly G 2018 Seasonal impact of regional outdoor biomass burning on air pollution in three Indian cities: Delhi, Bengaluru, and Pune *Atmos. Environ.* **172** 83–92 Online: https://doi.org/10.1016/j.atmosenv.2017.10.024

McCarty J L, Korontzi S, Justice C O and Loboda T 2009 The spatial and temporal distribution of crop residue burning in the contiguous United States *Sci. Total Environ.* **407** 5701–12 Online: http://dx.doi.org/10.1016/j.scitotenv.2009.07.009

McCarty J L, Loboda T and Trigg S 2008 A hybrid remote sensing approach to quantifying crop residue burning in the United States *Appl. Eng. Agric.* **24** 515–27

Mehta C R, Senthilkumar T, Scientist S and Singh K K 2014 *Trends of Agricultural Mechanization in India. CSAM Policy Brief.* Online: http://www.un-csam.org/publication/PB201402.pdf

Oliva P and Schroeder W 2015 Assessment of VIIRS 375m active fire detection product for direct burned area mapping *Remote Sens. Environ.* **160** 144–55 Online: http://dx.doi.org/10.1016/j.rse.2015.01.010

PRSC 2015 Monitoring Residue Burning Satellite Remote Sensing Online: http://www.ppcb.gov.in/Attachments/Reports and Documents/StudyReport.pdf

Randerson J T, Chen Y, Van Der Werf G R, Rogers B M and Morton D C 2012 Global burned area and biomass burning emissions from small fires *J. Geophys. Res. Biogeosciences* **117** Online: https://doi.org/10.1029/2012JG002128

Sharma A R, Kharol S K, Badarinath K V S and Singh D 2010 Impact of agriculture crop residue burning on atmospheric aerosol loading - A study over Punjab State, India *Ann. Geophys.* **28** 367–79 Online: https://doi.org/10.5194/angeo-28-367-2010

Strauss M 2017 Planet Earth to get a daily selfie *Science.* **355** 782–3 Online: https://doi.org/10.1126/science.355.6327.782

Thumaty K C, Rodda S R, Singhal J, Gopalakrishnan R, Jha C S, Parsi G D and Dadhwal V K 2015 Spatio-temporal characterization of agriculture residue burning in Punjab and Haryana, India, using MODIS and Suomi NPP VIIRS data *Curr. Sci.* **109** 1850–4 Online: https://doi.org/10.18520/v109/i10/1850-1855

United Nations 2015 *World Population Prospects: The 2015 Revision, Key Findings and Advance Tables. Working Paper No. ESA/P/WP.241.* Online: https://esa.un.org/unpd/wpp/publications/files/key_findings_wpp_2015.pdf

Vadrevu K P, Ellicott E, Badarinath K V S and Vermote E 2011 MODIS derived fire characteristics and aerosol optical depth variations during the agricultural residue burning season, north India *Environ. Pollut.* **159** 1560–9 Online: https://doi.org/10.1016/j.envpol.2011.03.001

van der Werf G R, Randerson J T, Giglio L, van Leeuwen T T, Chen Y, Rogers B M, Mu M, van Marle M J E, Morton D C, Collatz G J, Yokelson R J and Kasibhatla P S 2017 Global fire emissions estimates during 1997–2016 *Earth Syst. Sci. Data* **9** 697–720 Online: https://www.earth-syst-sci-data.net/9/697/2017/

Wiedinmyer C, Akagi S K, Yokelson R J, Emmons L K, Orlando J J and Soja A J 2011 The Fire INventory from NCAR (FINN): a high resolution global model to estimate the emissions from open burning *Geosci. Model Dev.* **4** 625–41 Online: https://doi.org/10.5194/gmd-4-625-2011

Yadav M, Prawasi R, Jangra S, Rana P, Kumari K, Lal S, Jakhar K, Sharma S and Hooda R S 2014a Monitoring seasonal progress of rice stubble burning in major rice growing districts of Haryana, India, using multidate AWiFS data *Int. Arch. Photogramm. Remote Sens. Spat. Inf. Sci.* **XL-8** 1003–9 Online: https://www.int-arch-photogramm-remote-sens-spatial-inf-sci.net/XL-8/1003/2014/isprsarchives-XL-8-1003-2014.pdf

Yadav M, Sharma M P, Prawasi R, Khichi R, Kumar P, Mandal V P, Salim A and Hooda R S 2014b Estimation of Wheat/Rice Residue Burning Areas in Major Districts of Haryana, India, Using Remote Sensing Data *J. Indian Soc. Remote Sens.* **42** 343–52 Online: https://doi.org/10.1007/s12524-013-0330-z

Zhang T, Wooster M J, de Jong M C and Xu W 2018 How Well Does the “Small Fire Boost” Methodology Used within the GFED4.1s Fire Emissions Database Represent the Timing, Location and Magnitude of Agricultural Burning? *Remote Sens.* **10** 823 Online: https://doi.org/10.3390/rs10060823

Zhu C, Kobayashi H, Kanaya Y and Saito M 2017 Size-dependent validation of MODIS MCD64A1 burned area over six vegetation types in boreal Eurasia: Large underestimation in croplands *Sci. Rep.* **7** 1–9 Online: https://doi.org/10.1038/s41598-017-03739-0

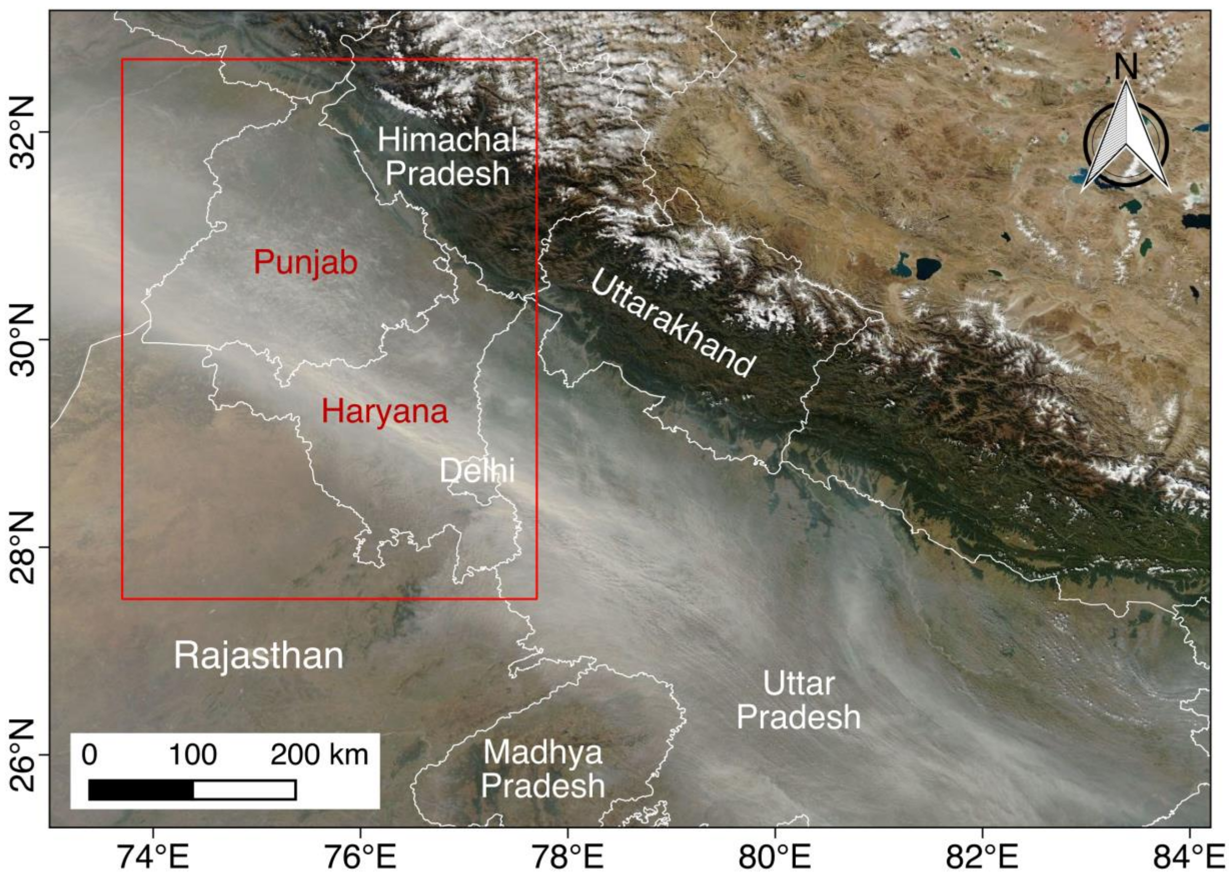

Figure 1. Example of thick haze over northern India during the post-monsoon burning season: True color MODIS/Aqua on November 6, 2016 (NASA Worldview). The study area, which consists of two agricultural states Punjab and Haryana, is bounded by a red box.

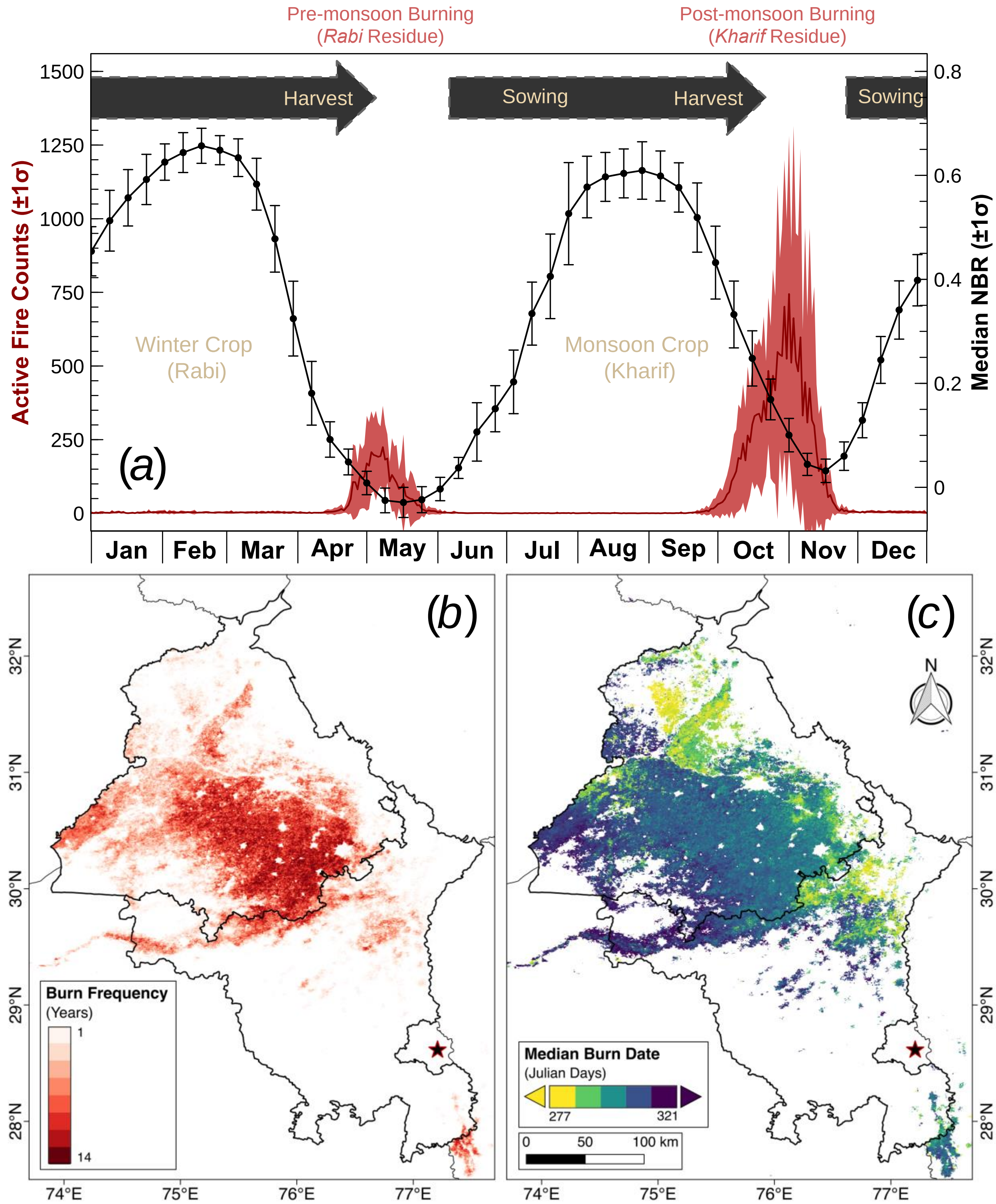

Figure 2. Spatio-temporal overview of agricultural burning in northwestern India: (*a*) The double crop-fire cycle, following Vadrevu et al. (2011), using daily MODIS fire counts and 8-day composite median NBR, with ±1σ envelopes, in Punjab and Haryana, 2003-2016. Post-monsoon (October-November) (*b*) burn frequency and (*c*) median burn date based on $BA_{MCD64A1}$. The star denotes the location of New Delhi.

Table 1. Post-monsoon CO_2, CO, OC, and BC emissions over Punjab and Haryana from 2003-2016 for five global fire emissions inventories. Agricultural-only emissions are denoted in italics.

	Inventory	**CO_2**	**CO**	**OC**	**BC**	*% Punjab*
		Gg (±1σ)				
Bottom-up (derived from burned area)	GFEDv4s	6325 (2204)	406 (142)	9 (3)	3 (1)	77-85
		6397 (2201)	*405 (142)*	*9 (3)*	*3 (1)*	*77-85*
	FINNv1.5	14950 (2841)	1061 (198)	32 (6)	6.6 (1.4)	76-86
		14442 (2648)	*1043 (191)*	*31 (6)*	*6.5 (1.2)*	*76-85*
Top-down (derived from fire energy)	GFASv1.2	3460 (671)	243 (47)	11 (2)	1.1 (0.2)	82-89
	QFEDv2.5r1	7757 (1486)	313 (60)	29 (6)	4.2 (0.8)	81-89
	FEERv1.0-G1.2	38257 (7342)	2473 (473)	108 (21)	11 (2.1)	78-87
CV (%)		100	104	107	74	

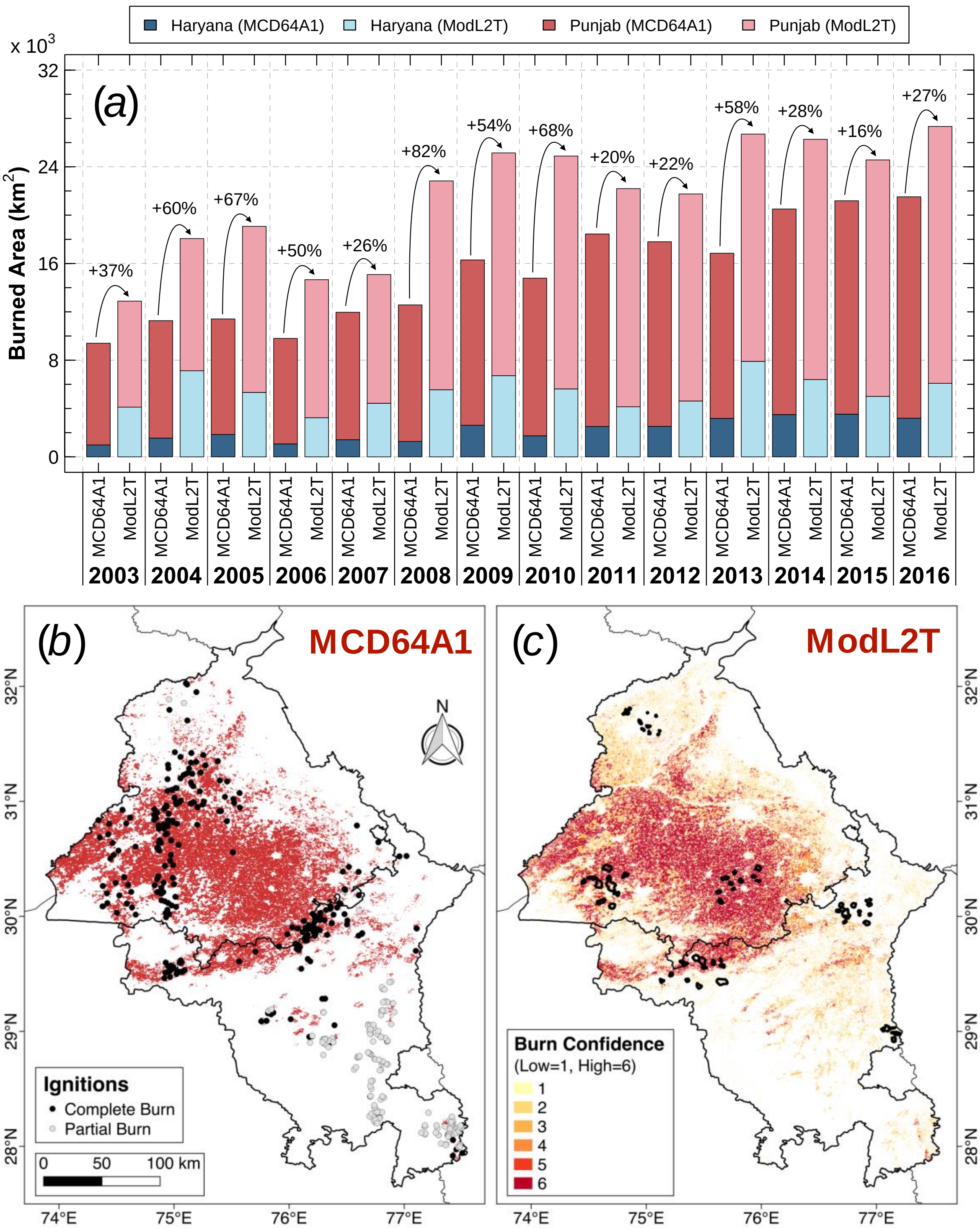

Figure 3. MCD64A1 and ModL2T burned area: (*a*) $BA_{MCD64A1}$ and BA_{ModL2T} in Punjab (red shades) and Haryana (blue shades) during post-monsoon (October-November), 2003-2016. The ModL2T algorithm estimates 44 ± 21% higher post-monsoon burned area in Punjab and Haryana than MCD64A1. The curved arrows denote the relative boost in burned area mapped by ModL2T compared to MCD64A1. (*b*) $BA_{MCD64A1}$ and (*c*) classification confidence (Low = 1, High = 6) for BA_{ModL2T} in Haryana and Punjab, post-monsoon (October-November) in 2016. Ignitions identified from fine-resolution imagery, from 2010-2016 are denoted as black (complete burns) and gray (partial burns) circles in (*b*). The locations of the villages surveyed in Punjab and Haryana in 2016 are shown as black polygons in (*c*). The star denotes the location of New Delhi.

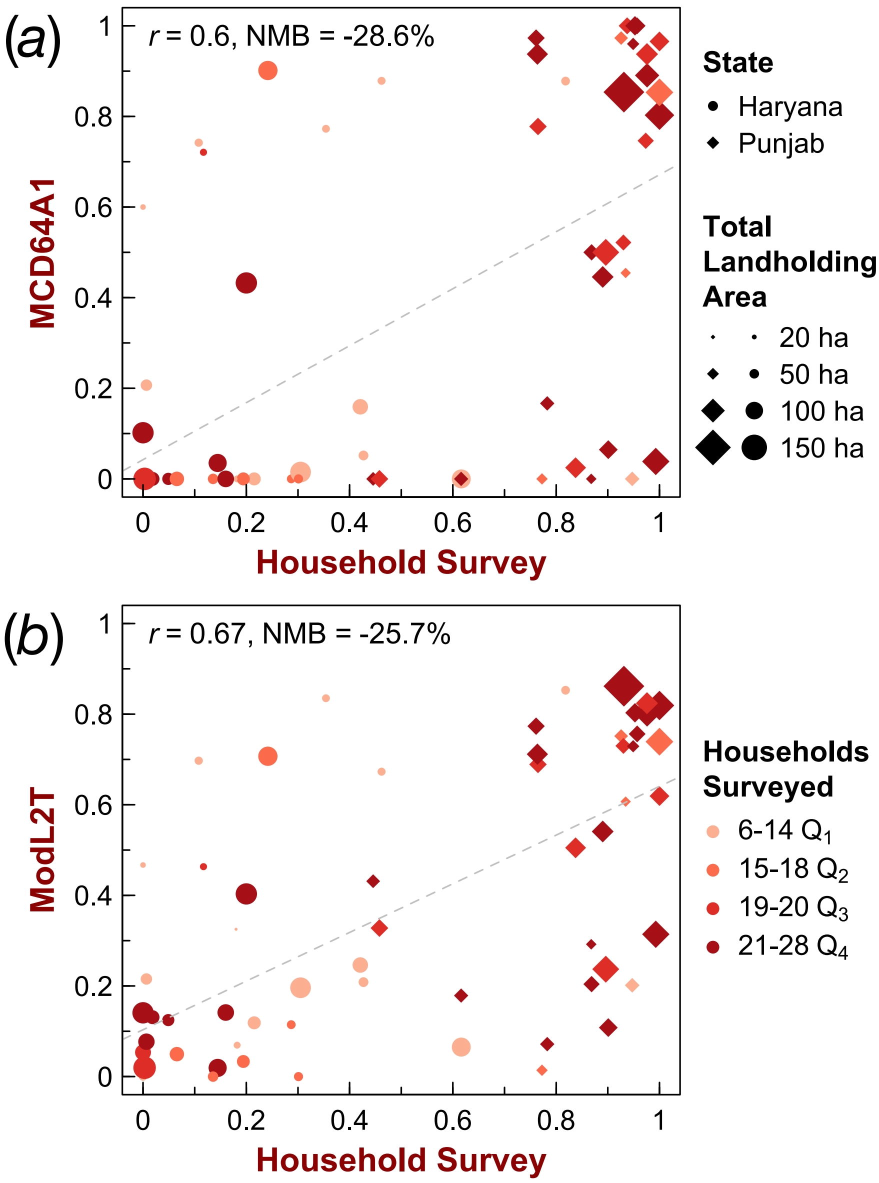

Figure 4. Validation of satellite-derived burned area using household surveys: comparison of % burning activity, normalized by landholding size, and % burned area from (*a*) MCD64A1 and (*b*) ModL2T in 30 Punjab (diamonds) and 32 Haryana (circles) villages during post-monsoon (October-November) in 2016. Inset shows the correlation coefficient ($p < 0.05$), weighted by total landholding area from the household survey, and normalized mean bias (NMB). The size of the markers denotes the total landholding area (in hectares), and the color denotes the quartile of the number of households surveyed per village. The locations of the 62 surveyed villages are shown in Figure 3c.

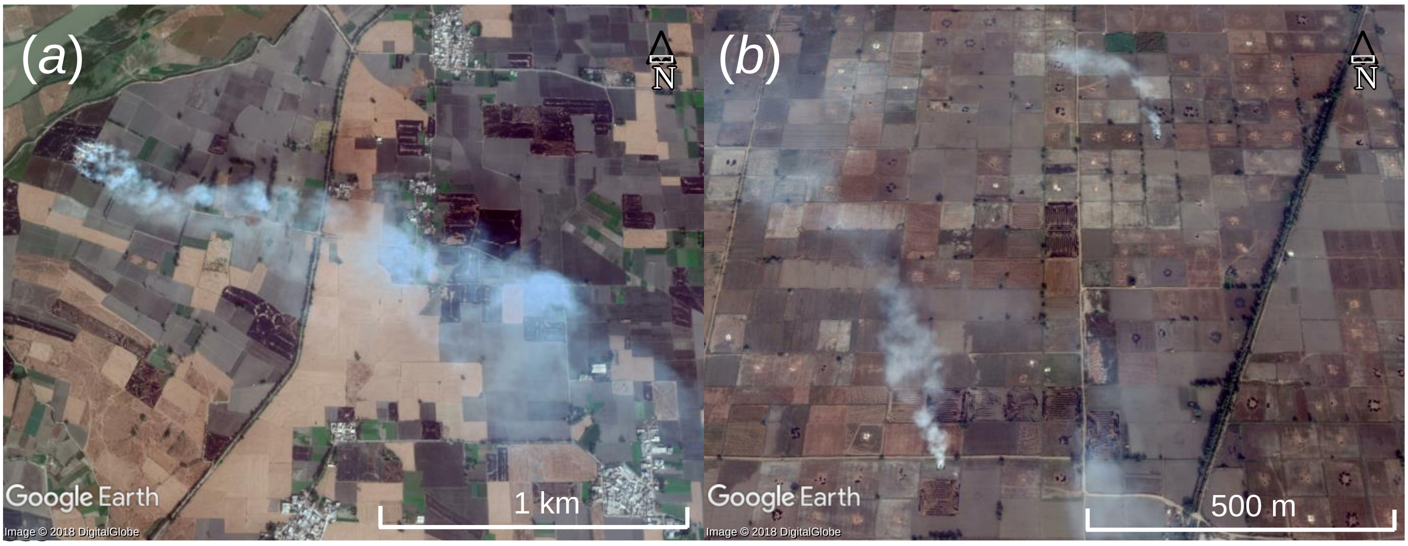

Figure 5. Two crop residue burning practices: Fine-resolution (<5 m) Google Earth DigitalGlobe historical imagery of smoke and burn scars from crop residue burning in (*a*) central-northern Punjab (complete burns) and (*b*) central Haryana (primarily partial burns) in November 2016.

Table 2. Validation of MODIS MxD14A1 active fires using geolocations of ignitions identified from fine-resolution imagery. The spatial distribution of the ignitions is shown in Figure 3b.

Year	**Ignitions**			**MxD14A1**, co-location with ignition pixels					
	total ignitions (1-km pixels)			*same day, %*			*same season, %*		
	Partial	Complete	Total	Partial	Complete	Total	Partial	Complete	Total
2010	78 (55)	15 (12)	93 (67)	0	0	0	0	50	9
2011	52 (39)	15 (11)	67 (50)	0	45	10	0	64	14
2012	9 (7)	2 (1)	11 (8)	0	0	0	0	100	12
2013	3 (2)	63 (58)	66 (60)	0	2	2	0	38	37
2014	6 (3)	86 (72)	92 (75)	0	11	11	0	42	40
2015	32 (27)	25 (19)	57 (46)	0	11	4	4	32	15
2016	42 (30)	96 (77)	138 (107)	0	5	4	10	36	29
All	222 (163)	302 (250)	524 (413)	0	8	5	2	40	25

Table 3. Crop residue burning related to methods of rice harvesting across eight districts in Punjab and Haryana from household survey data in 2016.

State	Districts	Crop residue burning				*n*
		Combine Harvester	*Partially Mechanical*	*Manual*	*Both Manual and Mechanical*	
Punjab	Amritsar, Bathinda, Muktsar, Sangrur	466 (87%)	3 (43%)	7 (30%)	19 (54%)	601
Haryana	Fatehabad, Sirsa, Kurukshetra, Sonipat	62 (32%)	1 (25%)	7 (5%)	4 (15%)	371
	Total	**528 (72%)**	**4 (36%)**	**14 (8%)**	**23 (38%)**	**972**